Original Research Article

High plasticity of an iron aluminide-based material at low temperatures

Abstract

High-quality compacts from atomized Fe-30.8Al-0.35Zr-0.11B (at.%) powder were prepared using spark plasma sintering method. High plasticity (plastic strain more than 30% without failure) was observed in compressive tests at room temperature and at 77 K. Electron microscopy observations revealed the dominating role of dislocation motion in compression at low temperatures. The ductility measured at tensile tests, on the other hand, was only about 1% with a typical brittle failure. Elastic properties (Young's and shear moduli data) of the sintered material were measured in the temperature range from room temperature to 80 K.

Keywords:

Intermetallics; Powder metallurgy; Mechanical properties; Scanning electron microscopy, SEM; Transmission electron microscopy, TEM;

1. Introduction

Iron aluminides based on FeAl and Fe_3Al have been widely studied, mainly because of their excellent high temperature oxidation and corrosion properties. However, poor formability and ductility, particularly at room temperature, present a serious problem for the industrial application of these materials. There are many factors influencing the plasticity of these materials (e.g. testing environment, Al content, substitutional alloying, dispersed particles, grain size, quenched-in vacancies) [1-5].

In previous unpublished work we performed a cryo-milling of an atomized powder of an iron aluminide-based alloy in liquid nitrogen at 77 K and compared the microstructure of powder particles before and after milling. We observed clear signs of high intrinsic plasticity of the milled polycrystalline powder particles and no signs of brittle cracking (see below).

Spark plasma sintering (SPS) is a rapid consolidation technique that uses pulsed direct electric current to generate heat and uniaxial pressure. When SPS is applied to powders, densification can be achieved at significantly lower temperatures and shorter times than conventional sintering, thereby limiting grain growth and preserving the fine microstructure [6].

The SPS procedure is often used to sinter powder that has been prepared by mechanical alloying of elemental powders or by milling a powder prepared by gas atomization of an alloy under argon (to achieve mechanical activation of particle surfaces and grain refinement). In both cases the milled powder is highly reactive with a heavily deformed microstructure. By sintering of such a powder we can expect a bulk material with improved hardness and strength [7].

The previous studies confirmed the advantages of the SPS-method by successful fabrication of dense fine grained Fe-Al materials with promising mechanical properties [7-10].

In the present work we exploit the low temperature plasticity of the feedstock powder for the preparation of a dense bulk material with similar unusual mechanical properties at low temperatures. The primary scope of this study is to report and discuss the observed high plasticity of this material at room temperature and at 77 K.

2. Experimental

The feedstock powder was prepared using atomization in argon by LERMPS/PERSEE, France. The size distribution of spherical particles was characterized by d_{10} = 13.7 μm, d_{50} = 29.0 μm, d_{90} = 51.2 μm as determined by laser granulometry. The chemical analysis of Al, B and Zr in the atomized powder was performed by ICP-OES method using an Iris Intrepid HR, Thermo Scientific, the analysis of C was made using absorption spectrometer LECO CS-444: the analysis of O was performed using an absorption spectrometer LECO TC-300.
The atomized powder was consolidated using two different devices: SPS 10-4 apparatus (Thermal Technology LLC) and FCT HP D10 apparatus. The graphite die of 20 mm (50 mm for FCT machine) in diameter was internally protected from the loaded powder by a graphite foil or tungsten foil that can prevent contamination by carbon. The powder in the die was heated to the sintering temperature of 1100 ^{o}C (1000 ^{o}C) with a heating rate of 200 K/min (100 K/min). A pressure of 70 MPa (48 MPa) was applied and maintained until completion of sintering. The dwell time at 1100 ^{o}C (1000 ^{o}C) was 3 min (30 min), followed by fast cooling (200 K/min) to 850 ^{o}C and then by slower cooling (100 K/min) to room temperature. This choice of sintering parameters is close to conditions of the SPS used in [10]. The dimensions of the sintered cylindrical samples were Ø 19 mm x 5 mm (Ø 49 mm x 30 mm).
The microstructure and phase composition of the sintered samples were characterized by X-ray diffraction (XRD), scanning electron microscopy (SEM) with electron back scatter diffraction (EBSD) and by transmission electron microscopy (TEM). XRD measurements were performed using a Bragg Brentano θ/2θ Bruker X-ray diffractometer, type D8 (Cu K_{α} and Co $K_{\alpha 1}$ radiation). SEM observations were performed using Zeiss Auriga Compact Crossbeam$^{®}$ microscope equipped with EDAX EBSD camera DigiView 5. The identification and visualization of grains was made using the EBSD method by orientation imaging maps. TEM specimens were prepared by mechanical grinding and polishing of thin targets to a thickness of about 100 μm, and thinning to electron transparency using a Struers Tenupol 2 twin jet electrolytic polisher. TEM observations were performed using a JEOL 2000FX electron microscope.
Mechanical properties of the feedstock powder were characterized using a Qness Q10A microhardness tester with Vickers load of 25 gram. The same measurements were made on sintered samples in different parts of cylindrical SPS discs, parallel and perpendicular to the cylindrical axis. Cuboid-shaped compressive samples, typically of 4.9 x 3.5 x 3.5 mm^{3}, were sectioned by diamond saw from the SPS disk parallel and perpendicular to the axis of the disk. Samples for tensile tests with round cross-section (Ø4 mm) and threaded shoulders were cut parallel to the axis of the bigger SPS-disk. The tests were performed in air at RT and in liquid nitrogen at 77 K with an initial strain rate of 1.0 x 10^{-3} s^{-1}, using an Instron 1186 universal testing machine.
The elastic properties (Young's and shear moduli) of the examined material were measured by a combination of two ultrasonic methods: the pulse-echo method [11] and the resonant ultrasound spectroscopy [12,13]. For the ultrasonic measurements, a perfect cuboid sample of dimensions approximately 2.0 x 3.0 x 4.5 mm^{3} was used. Firstly, the velocities of longitudinal and shear ultrasonic waves in three directions perpendicular to the faces of the sample were measured at RT (295 K) using the pulse-echo (P-E) method, in order to confirm the assumed elastic isotropy of the compact. The outputs of the P-E method also enabled direct calculation of the Young's modulus E and the shear modulus G. These values were then used as initial approximations for the inverse procedure in the resonant ultrasound spectroscopy (RUS) method. Secondly, the RUS method was applied to determine accurately the elastic constants in the temperature range from RT to 80 K.

3. Results

3.1. Material characterization

The results of the chemical analysis of the atomized powder are displayed in Table 1.

Table 1
Chemical composition of the atomized powder.

element	Fe	Al	B	C	O	Zr
at.%	bal.	30.8(2)	0.109(5)	0.059(1)	0.132(3)	0.355(5)

The XRD pattern (the red curve in Fig. 1) of the as-received atomized powder showed the presence of the ordered B2 phase[*]. The Rietveld profile analysis of the XRD powder pattern revealed about 0.6wt.% of the λ_1 hexagonal C14 Laves phase in the atomized powder, in agreement with former observations [14,15].

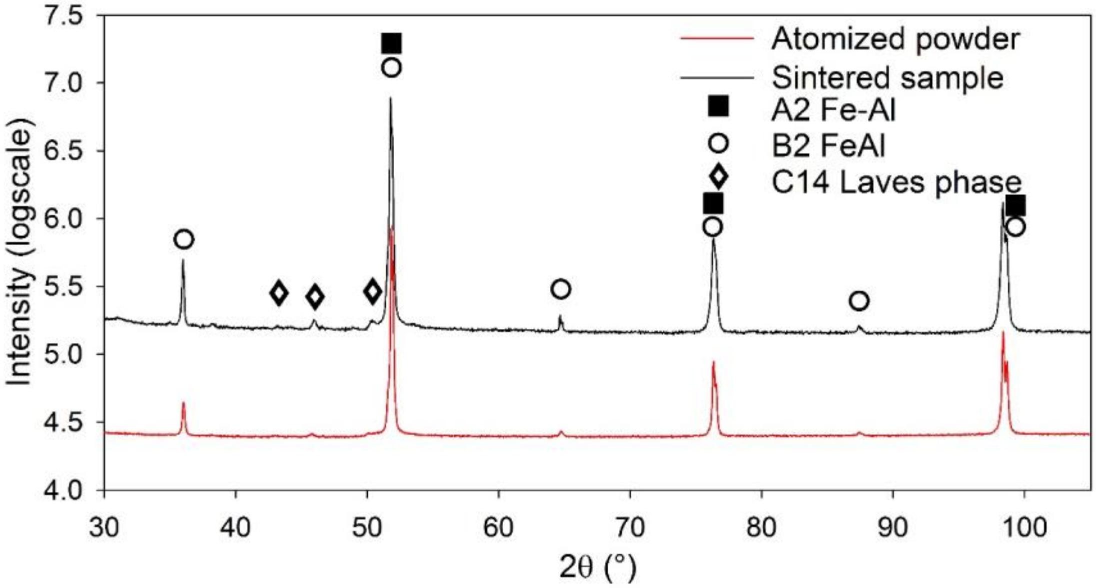

Fig. 1 XRD patterns of the atomized powder and sintered sample.

The microstructure of individual atomized powder particles was successfully determined by SEM and EBSD methods (Fig. 2). Some of the particles have a spherical cavity inside (Fig. 2 below), i.e. these particles solidified as bubbles in argon during atomization process. The microstructure of atomized powder particles, which were mechanically activated by milling at 77 K, is dramatically changed and shows clear signs of the intrinsic low temperature plasticity (i.e. plastic compressive and shear straining) (Fig. 3). The grains were identified as heavily strained disordered A2 (bcc) structure. The A2 structure (and the absenting B2 long range ordered phase) was confirmed also by XRD measurement.

---

[*] The fully developed $D0_3$ equilibrium structure with fcc Bravais lattice and doubled lattice parameter (a = 0.57914(2) nm) was observed after annealing of the powder for 408 h at 420 °C under an argon atmosphere.

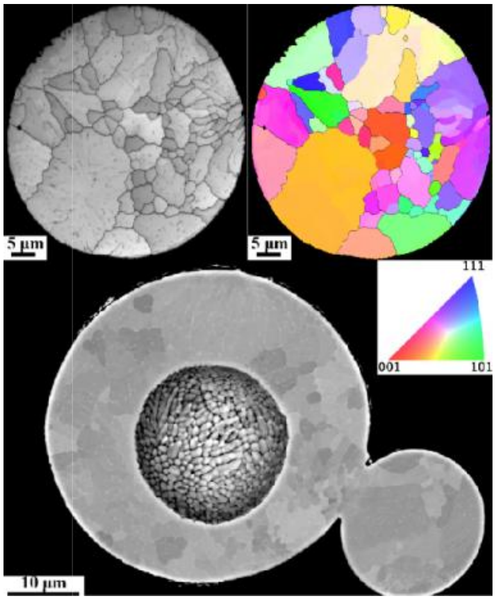

Fig. 2 The microstructure of an atomized powder particle observed by EBSD method (image quality map and orientation imaging map – upper image) and a particle with spherical cavity (SEM channeling contrast - bottom).

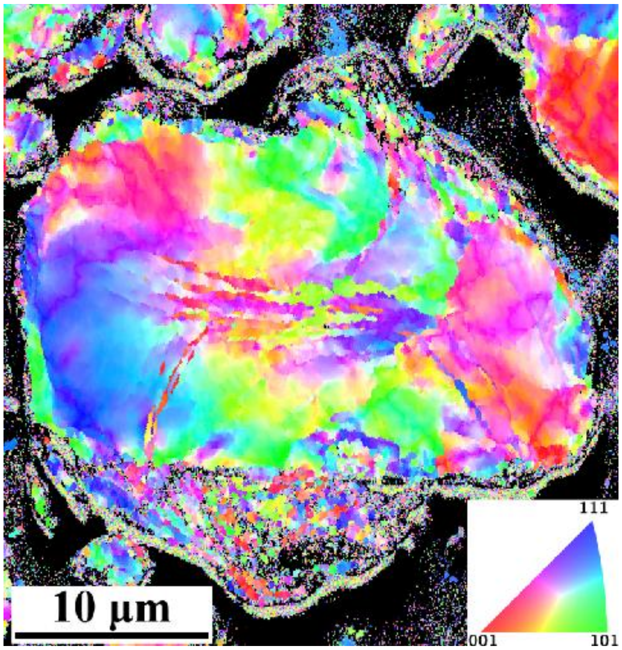

Fig. 3 Orientation imaging map of a cryo-milled (77 K) powder particle with the disordered A2 (bcc) structure.

Inspection of all sintered samples by electron microscopy revealed fully dense microstructure without any remarkable porosity. The sintered microstructure resembles the microstructure of atomized particles with very similar grains of the ordered B2 structure (Fig. 4).

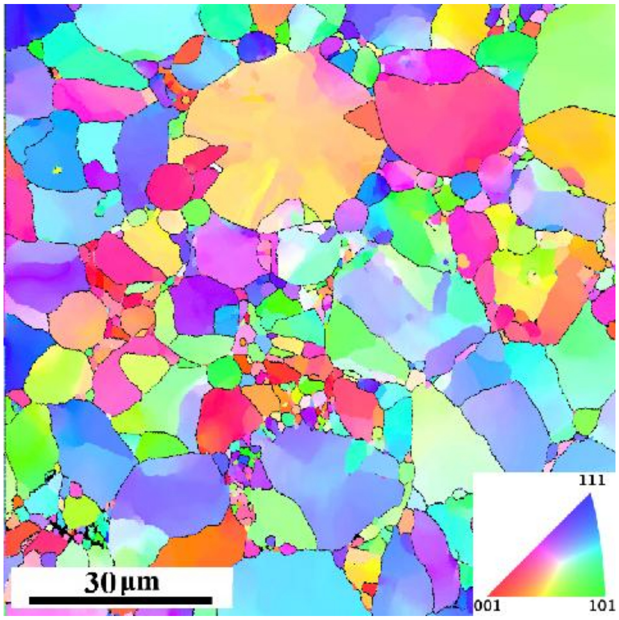

Fig. 4 Orientation imaging map of the sintered bulk material with the ordered B2 structure.

The sintered microstructure contains additionally also some new fine grains filling up the volume among original powder particles. The fine grains must have grown during the sintering process. The resulting microstructure has therefore a bimodal or multimodal distribution of grain sizes. XRD pattern of the sintered material (see Fig. 1) showed again the presence of the ordered B2 phase with small amount of the λ_1 hexagonal C14 Laves phase. Note that surface of several sintered samples was in contact with the graphite foil during the SPS process. It resulted in the formation of κ-$Fe_3AlC_{0.5}$ carbide particles extending several micrometers deep into the sintered material. Substitution of the graphite foil by the tungsten foil fully prevented the formation of the carbide.

3.2. Deformation behavior

Mechanical properties were studied using microhardness measurements at room temperature (RT) and using both compression and tensile tests at RT and 77 K.

The results of all microhardness measurements are summarized in Table 2. As can be seen from measured values of SPS-disks and their standard deviations the bulk material is homogeneous in the whole volume and the sintering process did not lead to a measurable deviation from microhardness of the feedstock powder particles.

Table 2

Microhardness HV 0.025 of powder particles and sintered materials.

	HV 0.025
atomized powder	380 ± 20
SPS bulk	370 ± 15

True stress vs logarithmic plastic strain curves are shown in Fig. 5, the yield strength, maximum strength and logarithmic plastic strain values with their standard deviations are summarized in Table 3.

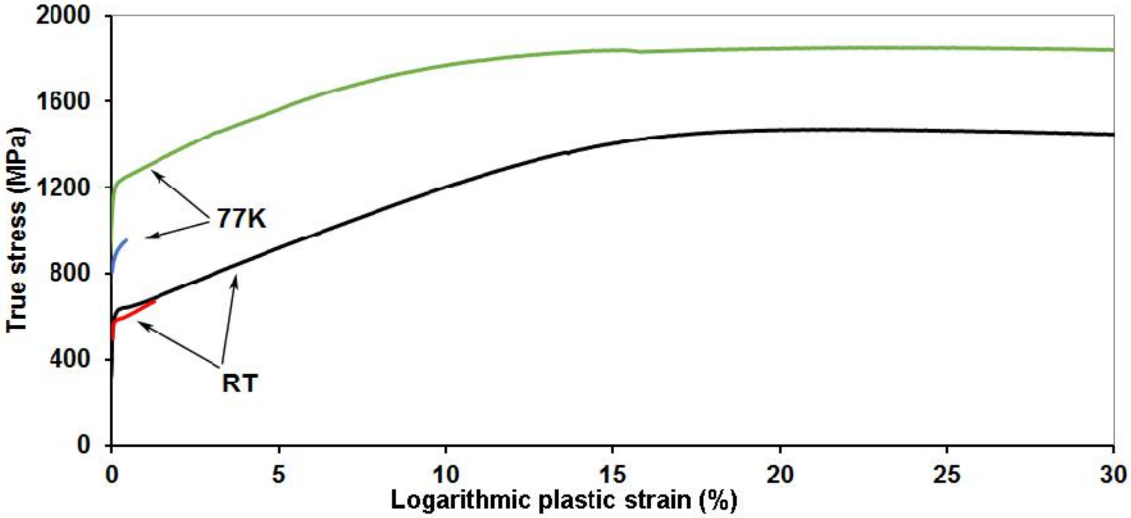

Fig. 5 Compressive (black and green) and tensile (red and blue) true stress vs logarithmic plastic strain curves for the sintered bulk material at RT and 77 K.

The data in Table 3 represent behavior of four sets of three samples measured during compressive and tensile tests in air at RT and in liquid nitrogen at 77 K, irrespective how they were cut from SPS-disks.

Table 3

The yield strength σ_{02}, maximum strength σ_{max} and logarithmic plastic strain of the sintered bulk material in air at RT and in liquid nitrogen at 77 K.

temperature	σ_{02} (MPa) (compression, tension)	σ_{max} (MPa) (compression, tension)	Logarithmic plastic strain (%) (compression, tension)
RT	630 ± 10, 590 ± 10	1530 ± 60, 660 ± 10	> 30, 1.2 ± 0.1
77 K	1215 ± 15, 920 ± 10	1850 ± 10, 950 ± 10	> 30, 0.4 ± 0.1

Note the relatively very good reproducibility of all parameters in Table 3 showing stability of the bulk material against variation of the SPS conditions. Substantial is the difference between plasticity of the material in compression and in tension.

3.3. Dislocations in compression and fracture in tension

The transmission electron microscopy (Fig. 6) of the studied bulk material revealed the following. In the as received material there is a very low dislocation density and a network of λ_1 Laves phase particles in B2 matrix grains (Fig. 6a). The material after compressive test at RT displays an inhomogeneous tangle of dislocations (Fig. 6b). Signs of recovery were detected at higher magnifications, i.e. cells with low dislocation density surrounded by cell walls with high dislocation density (see Fig. 7). This is not the case of material compressed at 77 K, there is only high density of homogeneously distributed dislocations with the exception of apparently non-deformed particles (Fig. 6c).

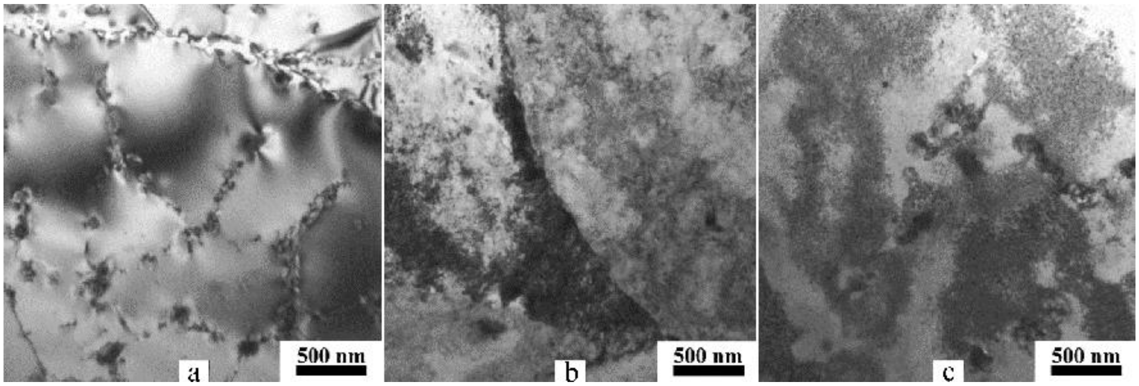

Fig. 6 TEM images of the sintered material: (a) as received; (b) after compressive test at RT; (c) after compressive test at 77 K.

The SEM micrographs of the fracture surface after tensile test show that the fracture occurred in a brittle manner with nearly planar fracture surface perpendicular to the tensile stress through a combination of interparticle and intergranular decohesion and also transgranular cleavage (see Fig. 8).

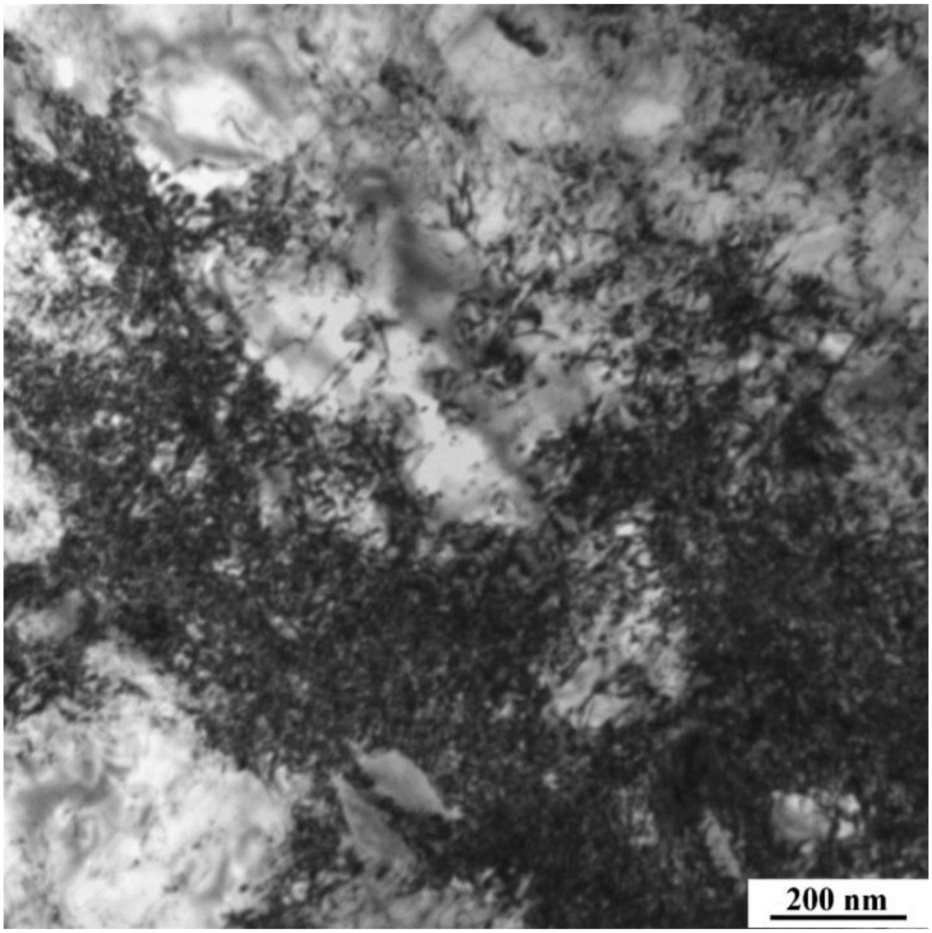

Fig. 7 TEM image of the sintered material after compressive test at RT.

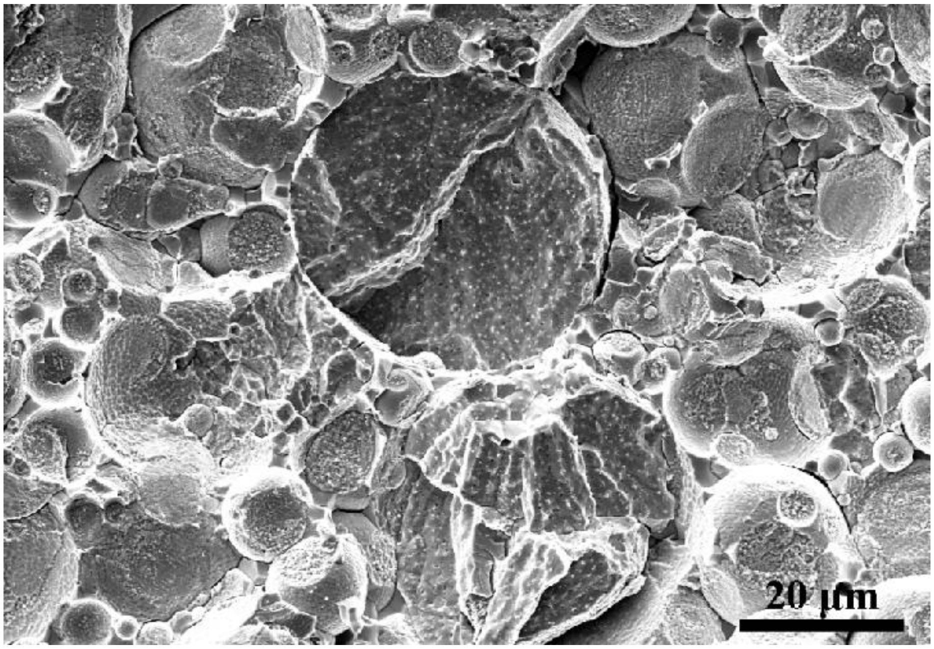

Fig. 8 SEM image of the fracture surface after tensile test at RT.

3.4. Elastic moduli

The density of the bulk material was determined from volume and mass of cuboid-shaped samples. The obtained value of (6290 ± 20) kg.m^{-3}, used for the data processing, together with a very good transmission of ultrasonic wave through the samples, confirmed the homogeneity of the material and the absence of macroscopic defects and porosity. Because the resulting velocities determined by the pulse-echo method in three orthogonal directions did not mutually differ by more than 1.2 %, we concluded that the material is isotropic.

The RUS method is based on measurements of the resonant spectrum of free elastic vibrations of the sample, from which the elastic constants are then determined via an iterative inverse procedure [12]. The temperature dependence *E(T)* and *G(T)* is shown in Fig. 9, the elastic moduli data for temperatures of performed deformation tests are shown in Table 4.

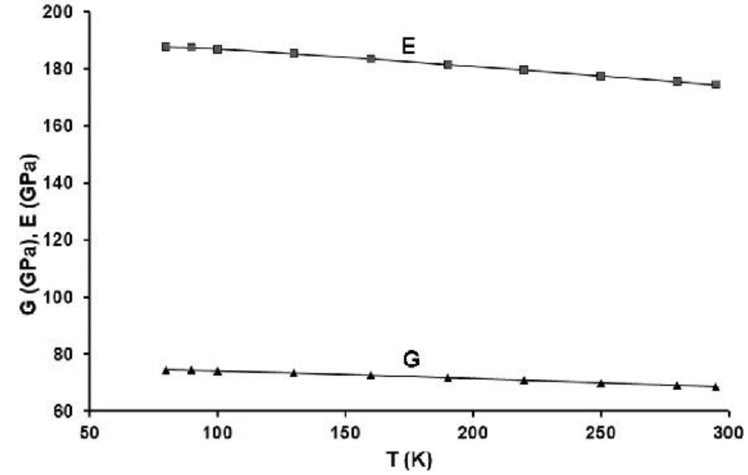

Fig. 9 Temperature dependence of the Young's modulus E and shear modulus G of the sintered material.

Homogeneous isotropic linear elastic materials have their elastic properties uniquely determined by two moduli. We calculated bulk modulus B according to the formula

$$B = \frac{EG}{3(3G - E)}$$

and the ratio B/G, introduced by Pugh [16] as a measure of ductility. If $B/G > 1.75$ the material is expected to deform in a plastic manner, lower values are associated with brittleness. Values of B and B/G for temperatures of performed deformation tests are listed in Table 4.

Table 4
Elastic moduli E, G, B and the ratio B/G of the sintered material at RT and 80 K.

temperature	E (GPa)	G (GPa)	B (GPa)	B/G
RT	174.4 ± 1.4	68.5 ± 0.3	128 ± 9	1.87 ± 0.12
80 K	187.7 ± 1.4	74.5 ± 0.3	132 ± 9	1.77 ± 0.12

The obtained data do not show any anomaly in the temperature dependence below RT and the Young's modulus at RT for our sintered material is higher or close above to values obtained in [17,18] for binary cast Fe-Al alloy with the same Al – concentration.

4. Discussion

The reason for different plasticity of our Fe-Al material in compression and in tension in air can be probably found in the following facts:

1) The environmental embrittlement considered as a major cause for the low ductility at RT in air [19], is related to high reactivity of Al atoms with the moisture in air. It creates hydrogen that penetrates as atomic hydrogen into material and very probably reduces the surface energy (the strength of interatomic bonds), which lowers the fracture toughness [20,21].

It seems that the hydrogen embrittlement is not in the game for deformation of our material. It may be due to good passivation of the surface of atomized particles that lowers hydrogen diffusivity in the sintered material. No ageing effect or a degradation of the powder has been observed after nearly three years. The improvement of plasticity in compression may be also due to the boron addition that increases grain boundary strength and there also may be an effect of Zr containing λ_1 particles or borides (comp. [2]).

2) The poor plasticity in tension is not an intrinsic behavior of the alloy (see dominating role of dislocation motion in compression), but it comes probably from nucleated nano/microcracks between sintered powder particles and/or cavities in originally partly hollow atomized particles. The microcracks open and propagate in the mode I (opening) in tension. Assuming a microcrack nucleates at yielding in tension, the crack propagates immediately after its nucleation when the stress for the crack propagation σ_f is lower than the yield stress σ_y (fracture in a brittle manner). On the other hand, when $\sigma_y < \sigma_f$, the crack propagation could occur only after additional plastic flow giving rise to work hardening, indicating that fracture in tension could be delayed in regions with finer grain size on the basis of the Hall-Petch relationship [22]. The finer was the grain size below the critical value, the greater was the ductility measured on polycrystalline isostructural NiAl samples at 400 ^{o}C [22].

The grain refinement can be made by milling of the powder, but this procedure produces also a significant strain hardening of milled particles. Their microhardness increases according to our measurements typically by about 60% and this strain hardening also leads to the increase of the yield strength of the sintered compact material. The milling procedure destroys the passivated surface of atomized particles and the environmental embrittlement of sintered material can be expected. This way we can therefore prepare a bulk material with a higher strength, but the material will be probably brittle not only in tension, but also in compression. In case of our measurements in compression the propagation of nucleated or pre-existing nano/microcracks does not occur, the internal stress does not reach a critical value σ_f for a fracture in a brittle manner, the sample in compression has the capacity for plastic deformation and even for the plastic flow (see Fig. 5) and the deformed sample obtains a typical barrel-shaped form.

3) The influence of temperature below RT on this behavior does not seem to be significant, the observed signs of dynamic recovery at RT only confirm the role of dislocations by deformation in compression. The measured shear modulus values scale also the resistance of the material to plastic deformation and relate this way to its hardness. The relative increase of the yield stress due to the lowering of temperature is naturally higher for both compressive and tensile tests in comparison with the relative increase of the shear modulus value. It is interesting that the corresponding absolute increase of the maximum flow stress σ_{max} in compression is the same as the increase of σ_{02} (and also σ_{max}) in tension. Pugh's values in Table 4 seem to be in agreement with observed plasticity in compression, but the application of this criterion to intermetallic compounds is probably less reliable than for pure metals.

4) Different slip directions in isostructural B2 alloys, the dislocation mobility and related ductility/brittleness are in general a complex problem [23]. It was shown that an interplay of elastic anisotropy of these cubic materials, displacement vectors of metastable planar faults and their energies govern the choice of the activated slip directions [23,24].

5. Conclusion

Very good plasticity at room temperature and at 77 K of the sintered FeAl-based material has been evidenced by EBSD of the cryo-milled feedstock atomized powder and in compression tests of the sintered material. The TEM observations confirm that dislocations enable the plastic flow in compression at low temperatures. The poor ductility in tension is not an intrinsic behavior of the alloy, but it results from the nucleation and opening of nano/microcracks between sintered powder particles and/or cavities in partly hollow atomized particles.

References

[1] D.J. Gaydosh, S.L. Draper, M.V. Nathal, Microstructure and tensile properties of Fe-40 at. pct. Al alloys with C, Zr, Hf, and B additions, Metall. Trans. A 20A (1989) 1701-1713.

[2] D.G. Morris, M.A.Morris-Muñoz, The influence of microstructure on the ductility of iron aluminides, Intermetallics 7 (1999) 1121-1129.

[3] D.G. Morris, M.A. Muñoz-Morris, J. Chao, Development of high strength, high ductility and high creep resistant iron aluminide, Intermetallics 12 (2004) 821-826.

[4] I. Baker, An overview of the mechanical properties of FeAl, Mater. Res. Soc. Symp. Proc. 1128 (2009) 1128-U02-01.

[5] M. Zamanzade, A. Barnoush, C. Motz, A review on the properties of iron aluminide intermetallics, Crystals 6 (2016) 10, http://dx.doi.org/10.3390/cryst6010010.

[6] R. Orrù, R. Licheri, A.M. Locci, A. Cincotti, G. Cao, Consolidation/synthesis of materials by electric current activated/assisted sintering, Mater. Sci. Eng. R 63 (2009) 127-287.

[7] G. Ji, F. Bernard, S. Launois, T. Grosdidier, Processing conditions, microstructure and mechanical properties of hetero-nanostructured ODS FeAl alloys produced by spark plasma sintering, Mater. Sci. Eng. A 559 (2013) 566-573.

[8] V. Šíma, P. Minárik, T. Chráska, Spark plasma sintering of ball milled and atomized powder based on Fe-Al, METAL 2015 – 24th International Conference on Metallurgy and Materials, Conference Proceedings, TANGER Ltd., 2015, pp. 1340-1345.

[9] V. Šíma, M. Cieslar, I. Çelikyürek, O. Torun, T. Chráska, Fully dense fine grained FeAl-based intermetallics prepared by spark plasma sintering method, Proceedings of the 8th Pacific Rim International Congress on Advanced Materials and Processing (PRICM8), F. Marquis (ed.), Wiley, 2013, pp. 361-368.

[10] T. Skiba, P. Haušild, M. Karlík, K. Vanmeensel, J. Vleugels, Mechanical properties of spark plasma sintered FeAl intermetallics, Intermetallics 18 (2010) 1410-1414.

[11] A.G. Every, W. Sachse, (eds.): Dynamic methods for measuring the elastic properties of solids, Handbook of elastic properties of solids, liquids and gases, Volume I., San Diego: Academic Press, 2001.

[12] R.G. Leisure, F.A. Willis, Resonant ultrasound spectroscopy, J. Phys.: Condens. Matter 9 (1997) 6001-6029.

[13] P. Sedlák, H. Seiner, J. Zídek, M. Janovská, M. Landa, Determination of all 21 independent elastic coefficients of generally anisotropic solids by resonant ultrasound spectroscopy: benchmark examples, Experimental Mechanics, 54 (2014) 1073-1085.

[14] D.G. Morris, I. Gutierrez-Urrutia, M.A. Muñoz-Morris, The high-temperature creep behavior of an Fe-Al-Zr alloy strengthened by intermetallic precipitates, Scripta Mater. 57 (2007) 449-452.

[15] F. Stein, G. Sauthoff, M. Palm, Phases and phase equilibria in the Fe-Al-Zr system, Z. Metallkd. 95 (2004) 469-485.

[16] S.F. Pugh, Relations between the elastic moduli and the plastic properties of polycrystalline pure metals, Phil. Mag. 45 (1954) 823-843.

[17] W. Köster, T. Gödecke, Physical measurements on iron-aluminium-alloys between 10 at. percent and 50 at. percent Al. 4. The modulus of elasticity of the alloys, Z. Metallkde. 73 (1982) 111-114.

[18] E. Frutos, D.G. Morris, M.A.Morris-Muñoz, Evaluation of elasic modulus and hardness of Fe-Al base intermetallics by nano-indentation techniques, Intermetallics 38 (2013) 1-3.

[19] C.T. Liu, E.H. Lee, C.G. McKamey, An environmental effect as the major cause for room-temperature embrittlement in FeAl, Scr. Met. 23 (1989) 875-880.

[20] M. Zamanzade, H. Vehoff, A. Barnoush, Cr effect on hydrogen embrittlement of iron aluminides, Acta Mater. 69 (2014) 210-223.

[21] M.H.Yoo, C.L. Fu, Cleavage fracture of ordered intermetallic alloys, Mater. Sci. Eng. A153 (1992) 470-478.

[22] E.M. Schulson, D.R. Barker, A brittle to ductile transition in NiAl of a critical grain size, Scr. Met. 17 (1983) 519-522.

[23] Yi-Shen Lin, M. Cak, V. Paidar, V. Vitek, Why is the slip direction different in different B2 alloys?, Acta Mater. 60 (2012) 881-888.

[24] G.H. Cao, A.T. Becker, D. Wu, L.S. Chumbley, T.A. Lograsso, A.M. Russel, K.A. Gschneidner Jr., Mechanical properties and determination of slip systems of the B2 YZn intermetallic compound, Acta Mater. 58 (2010) 4298-4304.